Characterization of a Site-Directed Mutant of Cytochrome b_5 Designed To Alter Axial Imidazole Ligand Plane Orientation†

Siddhartha Sarma,‡ Bindi Dangi,‡ ChunHua Yan,‡ Russell J. DiGate,‡ D. L. Banville,§ and R. D. Guiles*,‡

Department of Pharmaceutical Sciences, School of Pharmacy, University of Maryland at Baltimore, and Medical Biotechnology Center, Maryland Biotechnology Institute, University of Maryland, Baltimore, Maryland 21201, and Department of Medicinal Chemistry, Zeneca Pharmaceuticals, 1800 Concord Pike, Wilmington, Delaware 19897

Received July 26, 1996; Revised Manuscript Received February 25, 1997⊗

ABSTRACT: Mutants of cytochrome b_5 were designed to achieve reorientation of individual axial imidazole ligands. The orientation of the axial ligand planes is thought to modulate the reduction potential of bis(imidazole) axially ligated heme proteins. The A67V mutation achieved this goal through the substitution of a bulkier, hydrophobic ligand for a residue, in the sterically hindered hydrophobic heme binding pocket. Solution structures of mutant and wild-type proteins in the region of the mutation were calculated using restraints obtained from ^{1}H and ^{15}N 2D homonuclear and heteronuclear NMR spectra and ^{1}H−^{15}N 3D heteronuclear NMR spectra.. More than 10 restraints per residue were used in the refinement of both structures. Average local rmsd for 20 refined structures was 0.30 Å for the wild-type structure and 0.38 Å for the A67V mutant. The transfer of amide proton resonance assignments from wild-type to the mutant protein was achieved through overlays of ^{15}N−^{1}H heteronuclear correlation spectra of the reduced proteins. Side chain assignments and sequential assignments were established using conventional assignment strategies. Calculation of the orientation of the components of the anisotropic paramagnetic susceptibility tensor, using methods similar to procedures applied to the wild-type protein, shows that the orientation of the in-plane components are identical in the wild-type and mutant proteins. However, the orientation of the z-component of the susceptibility tensor calculated for the mutant protein differs by 17° for the A-form and by 11° for the B-form from the orientation calculated for the wild-type protein. The rotation of the *z*-component of the susceptibility tensor (toward the δ meso proton) is in the same direction and is of the same magnitude as the rotation of the H63 imidazole ring induced by mutation.

The cytochromes are a group of ubiquitous heme proteins that are involved in a number of important biological processes involving electron transfer (Mathews, 1985), such as xenobiotic and endobiotic metabolism (Guengrich, 1987), and bioenergetics in both respiration and photosynthesis (Diesenhofer, 1993). The bis(imidazole) cytochromes are a subclass of these electron transfer proteins containing imidazole ligands at both axial sites. This subclass of cytochromes spans an enormous range of redox potentials (e.g., 0 to +300 mV; Mathews, 1985). Factors that control bis(imidazole) cytochromes' electrochemical properties are not well understood. However, several hypotheses have been presented in an attempt to explain variation in the observed reduction potentials in terms of protein factors which control axial imidazole orientation (Walker *et al*., 1986) and local charge density (Cutler *et al*., 1989). Mutational studies described herein have been designed to evaluate factors which modulate bis(imidazole) cytochrome reduction potentials through site-directed mutagenesis in the heme binding pocket.

Previous studies directed at perturbing electrochemical properties have involved mutations that promote disruption of key hydrogen bonds and displacement of charged residues. It has been proposed that such interactions alter the stability of the higher oxidation state of the metal center and thereby regulate the reduction potential. Other mutational studies on the cytochrome b_5 system have involved replacement of one of the histidine axial ligands with a methionine to mimic *c*-type cytochromes. Such mutations have resulted in protein folding problems and drastic changes in reduction potentials. In some cases the mutations have conferred new properties to the system.

Mutations of other residues in the heme binding pocket to alter the orientation of the axial ligand (imidazole ring) planes have not been attempted. It is thought that the orientation of the planes of the axial ligands with respect to each other, in six-coordinate bis(imidazole) heme proteins, modulates the reduction potential (Safo *et al*., 1991; Walker *et al*., 1986; Scheidt *et al*., 1986).

Our interest lies in studying the protein factors that control heme reduction potential in rat cytochrome b_5. Although many species variants have been isolated and characterized [for a review see Mathews (1985)], the rat cytochrome b_5 is unique in that it has the maximum detectable heterogeneity in solution. It exists as a mixture of two forms (6:4 abundance ratio; other species exist in a ratio of 9:1 or higher) (Lee *et al*., 1990). The two forms of rat cytochrome b_5 differ by a 180° rotation of the heme in the binding pocket about an axis defined by the α and γ meso carbons (La Mar *et al*., 1981). Interestingly, the two forms differ in reduction potential by 27 mV (Walker *et al*., 1988). Our goal in this study has been to examine point mutations of rat cytochrome

† Supported by National Institutes of Health Grant DK 46510 (R.D.G.), and the School of Pharmacy of the University of Maryland at Baltimore.

* To whom correspondence should be addressed.
‡ University of Maryland.
§ Zeneca Pharmaceuticals.

⊗ Abstract published in *Advance ACS Abstracts,* April 15, 1997.

S0006-2960(96)01858-2 CCC: $14.00

b_5 that perturb the electrochemical properties of this protein and structurally characterize them using high-resolution NMR[1] methods. NMR methods provide a powerful tool for probing structure and structural changes induced by mutation. Heteronuclear methods using ^{15}N-enriched proteins greatly expand the range of possible NMR experiments. The NMR of the paramagnetic proteins has yielded additional insights into local changes in ligand orientation and the electronic structure. NMR methods are most suitable for this system because of the small size and high solubility of the protein. The availability of a synthetic gene that codes for the soluble heme binding domain of rat cytochrome b_5 (von Bodman *et al*., 1986) has enabled enrichment with NMR-active heteronuclei such as nitrogen-15 and carbon-13, which allows a wider range of experiments to be performed and simplifies the steps involved in structural characterization (Clore & Gronenborn, 1991; Bax & Grzeseik, 1993). NMR is also a powerful tool which is capable of characterizing the dynamic properties of various residues that line the heme binding pocket (Nirmala & Wagner, 1988; Palmer *et al*., 1991). Complete assignment of both oxidized and reduced forms of the A67V mutation using novel heteronuclear transfer methods has enabled us to accurately characterize the orientation of the paramagnetic susceptibility tensor. Accurate susceptibility tensors are known for very few systems, cytochrome b_5 (Keller & Wüthrich, 1972; Veitch *et al.*, 1990; Guiles *et al*., 1993) and cytochrome *c* (Feng *et al.*, 1990; Gao *et al.*, 1991) being two of them. Reorientation of the susceptibility tensor has also been used as a sensitive probe of changes in axial ligand orientation in studies of cytochrome *c* (Miriam & Roder, 1995) and myoglobin (Rajarathman *et al.*, 1993). Other high-resolution structural methods such as X-ray crystallography have not been useful for the rat cytochrome b_5 system because of the static disorder introduced by the two different conformations present in nearly equal abundance.

MATERIALS AND METHODS

Plasmid Construction and Mutagenesis. The synthetic gene coding for the soluble heme binding domain of the rat cytochrome b_5 in a pUC13 plasmid (von Bodman *et al.*, 1986) was subcloned into an overexpression vector, pET3C, an IPTG-inducible vector containing a T7 RNA polymerase promoter and a high-affinity ribosome binding site. Detailed properties of this expression vector have been described elsewhere (Studier *et al.*, 1990).

Reengineering of the plasmid was accomplished in the following manner. A unique *Nde*I restriction site at the initiation codon of the gene was introduced using PCR-mediated amplification (Saiki *et al.*, 1988). The amplified gene was then ligated into the pET3C vector using *Nde*I and *Eco*RI restriction sites. *Escherichia coli* strain BL-21 (PlysS) which has the T7 RNA polymerase gene in its chromosome under the control of a lac UV5 promoter was transformed with the pET3C vector containing the rat cytochrome b_5 gene. T7 RNA polymerase could then be expressed by the addition of IPTG to the media. The original coding sequence was confirmed following reengineering using Sanger chain termination methods (Sanger *et al*., 1977).

Site-directed mutagenesis was accomplished using methods described by Kunkel *et al.* (1987). The synthetic gene coding for the rat cytochrome b_5 protein was ligated into bacteriophage M13mp18 DNA using PstI and EcoRI restriction sites. The M13 bacteriophage was used to infect *Escherichia coli* CJ 236 in order to prepare single-stranded DNA containing deoxyuracil. This single-stranded DNA was used as a substrate for *in vitro* mutagenesis reactions. First, a unique NdeI restriction site was introduced at the initiation codon of the gene. Next, an oligonucleotide primer complementary to the sequence surrounding the codon coding for alanine 67 was used to affect a site-specific mutation from alanine 67 to valine 67. Single-stranded DNA templates were sequenced (Sanger *et al*., 1977) to verify the coding region region of the rat cytochrome b_5 gene for each mutant. The replicative form of the bacteriophage was then digested with *Nde*I and *Eco*RI restriction enzymes. The 330 bp fragment containing the coding region for A67V rat cytochrome b_5 was purified by electroelution and ligated into pET3C that was digested with the same restriction enzymes. Subsequently, the vector was used to transform *E. coli* strain BL-21 (PlysS). The G42A, L46N double mutant was prepared in a similar manner.

Purification and Labeling of Mutant Cytochromes b_5. Unlabeled A67V cytochrome b_5 was produced by growing cells at 37 °C in LB (10 g/L of tryptone, 5 g/L yeast extract, and 10 g/L NaCl) in the presence of ampicillin (100 mg/L). Induction of protein expression was achieved by the addition of 0.5 mM IPTG when the cells had grown to an O.D. of 0.6−0.8 at 590 nm. Cells were harvested 4 h after induction and disrupted by treatment with lysozyme. Roughly three-quarters of the protein was expressed in the apo form. Reconstitution of the holoprotein was accomplished using the procedure described by Walker *et al.* (1990). Estimates of A67V cytochrome b_5 in the lysates were performed by measuring absorbance at 413 nm assuming a millimolar absorptivity of 117 (Strittmatter & Velick, 1956). Purification of A67V rat cytochrome b_5 involved several modifications of the published procedure (von Bodman *et al*., 1986). The reconstituted crude extract was loaded onto a DEAE-Sephacel (Pharmacia) column that was previously equilibrated with Tris buffer (50 mM Tris, 1 mM EDTA, pH 8). The column was washed with two column volumes of buffer, and the protein was eluted with a 0−0.4 M KCl salt gradient (in Tris buffer). Following Amicon concentration of pooled fractions, the protein was loaded on a G-100 Sephadex (Pharmacia) column and eluted with Tris buffer. Cytochrome b_5 purified to apparent homogeneity was obtained following a final hydroxylapatite column. A gradient elution using 0−0.5 M $(NH_4)_2$ SO_4 was used in this final step. Fractions with a A_{413}/A_{280} ratio > 5.85 that showed a single band on gel electrophoresis were pooled together and dialyzed against 100 mM NH_4HCO_3, lyophillized and used in the biophysical studies described below. The above procedure yielded approximately 60 mg/L of pure protein using rich media.

[1] Abbreviations: NMR, nuclear magnetic resonance; A67V, alanine 67 → valine mutation; RNA, ribonucleic acid; PCR, polymerase chain reaction; DNA, deoxyribonucleic acid; IPTG, isopropyl thiogalactoside; DEAE, diethylaminoethyl; G42A, L46N, glycine 42 → alanine, leucine 46 → asparigine double mutation; TSP, sodium (trimethylsilyl)-propionate; NOE, nuclear Overhauser effect; DQFCOSY, 2D double-quantum-filtered correlated spectroscopy; TOCSY, 2D total correlation spectroscopy; NOESY, 2D nuclear Overhauser enhancement and exchange spectroscopy; HOHAHA, 2D homonuclear Hartmann−Hahn spectroscopy; HMQC, 2D heteronuclear multiple-quantum correlation spectroscopy; t_1, evolution time; t_2, evolution time (3D experiments) or data acquisition time (2D experiments); t_3, data acquisition time (3D experiments).

The change from a pUC13 plasmid to a pET3C plasmid (both IPTG-inducible plasmids) and a new host strain (PlysS) was accompanied by an increase in yield that is at least five times greater than that obtained in previously reported expression systems (von Bodman *et al.*, 1986, Guiles *et al.*, 1992). This system also allowed for the high-yield expression of mutants of rat cytochrome b_5. Uniformly ^{15}N-enriched A67V cytochrome b_5 was prepared by growing cells in M9 minimal media (McIntosh *et al*., 1987) in which $^{15}NH_4Cl$ (Cambridge Isotopes, 99% ^{15}N) was used as the sole source of nitrogen. Steps involved in purification were identical to those outlined above. Expression of protein in minimal media resulted in lower yields. In minimal media we obtained 40 mg/L pure protein.

Purification of a double mutant, G42A, L46N, was performed using an identical procedure. The stability and yields of this mutant were much lower, approximately 20 mg/L using rich culture media, than that of the A67V mutation. As a result detailed physical characterization of this mutant was not possible. However, as described in the following paper (Sarma *et al.*, 1997), estimates of the reduction potential were made on the basis of an irreversible cathodic wave in the cyclic voltammogram of the mutant protein.

NMR Sample Preparation. Samples for NMR experiments were prepared by dissolving purified A67V cytochrome b_5 in a 100 mM phosphate buffer, pH 7.2, prepared in 90% H_2O (10% D_2O). The pH was adjusted to 7.00 by the addition of small aliquots of 0.1 N NaOH. TSP [(trimethyl silyl)propionic acid] was added to a final concentration of 1 mM as an internal chemical shift standard, and the volume was adjusted to 0.5 mL. A67V ferri cytochrome b_5 concentrations were determined using a millimolar absorptivity of 117 at 413 nm. Optical spectra were recorded on a Shimadzu UV160u double-beam spectrometer. A final concentration of 4−7 mM was used in all NMR experiments. Samples of A67V ferro cytochrome b_5 were prepared by purging with nitrogen prior to reduction by the addition of solid sodium dithionite. A reducing atmosphere was maintained by sealing the NMR tube under vacuum with a gas−oxygen torch.

NMR Data Acquisition. NMR data were recorded on a Bruker AMX 500 spectrometer operating at a proton frequency of 500.13 MHz or a GE Omega PSG 600 spectrometer operating at a proton frequency of 599.71 MHz. All spectra were recorded in the phase-sensitive mode using the TPPI (Marion & Wüthrich, 1983) or States (States et al., 1982) method of quadrature detection. The sample temperature was maintained at 40 °C during all experiments. Relaxation delay times between 1 and 1.5 s were used in all experiments. Water suppression was achieved by using on resonance presaturation during the relaxation delay.

Two-Dimensional NMR Spectra. Two dimensional ^{1}H−^{1}H correlation DQFCOSY (Piantini *et al.*, 1982), and "clean" TOCSY (Greisinger *et al*., 1988) (50 and 70 ms mixing times) spectra using the MLEV-17 spin-lock sequence (Bax & Davis, 1985) were acquired at 500-MHz using the TPPI mode of quadrature detection. Homonuclear NOESY (Kumar *et al.*, 1980)(160 and 200 ms mixing times) spectra were acquired at 600 MHz using the States method of quadrature detection. Proton spectral widths of 7847 and 8733 Hz were employed at 500 and 600 MHz respectively.

Two-dimensional ^{1}H−^{15}N correlation spectra were acquired using the HMQC sequence (Bax *et al*., 1983) with proton and nitrogen spectral widths of 3846 and 1900 Hz respectively. All spectra were recorded with 512 t_1 increments to give a matrix of 1024 complex t_2 points × 512 real t_1 points. Nitrogen-15 chemical shifts were referenced to an external $^{15}NH_4Cl$ reference standard (WGN-01) obtained from Wilmad Glass Co. and reported relative to liquid ammonia. Broad-band ^{15}N decoupling during proton acquisition was achieved using the Waltz-16 sequence (Shaka *et al.*, 1983). To optimize digitization the carrier was shifted to the center of the amide proton region following presaturation.

Three-Dimensional NMR Spectra. Heteronuclear 3D ^{15}N-filtered experiments were recorded in a manner that maximizes digital resolution (Kay *et al*., 1989) in all three dimensions. TPPI phase cycling was employed to obtain phase-sensitive absorption spectra. The 3D NOESY−HMQC spectrum (Marion *et al*., 1989a) was acquired with a mixing time of 150 ms. The 3D HOHAHA−HMQC (Marion *et al*., 1989b) spectrum was acquired with a 50 ms mixing period using the "clean" MLEV-17 mixing scheme. Sweep widths of 3846 Hz in F_3 (^{1}H), 1900 Hz in F_2 (^{15}N), and 8002 Hz in F_1 (^{1}H) were used for both the NOESY−HMQC and the HOHAHA−HMQC experiments. In each case 256 real t_1, 64 real t_2, and 1024 complex data points in t_3 were recorded.

Data Processing. All NMR data were processed on a Silicon Graphics workstation with Felix V2.3 (Biosym Technologies Inc.) software. A Gaussian filter with a line-broadening parameter of 6 Hz was applied in the acquired dimension for all 2D spectra. In the F_2 dimension a squared sine bell weighting function phase-shifted by 90° was applied to remove truncation artifacts. Similarly for the 3D NOESY−HMQC and 3D HOHAHA−HMQC a sine squared weighting function phase-shifted by 90° was applied in the F_1 dimension. Forward linear prediction (Olejniczak & Eaton, 1990) was used to extend the time domain data in F_2 and F_1 in the three dimensional data sets by a third of the acquired points. Interactive phase correction was applied in all dimensions. Two-dimensional data sets were zero-filled in both dimensions to yield final matrices of 2048 × 2048 real data points. Three dimensional data sets were zero-filled once in F_1 and F_3 to yield final real matrices of 512 × 512 × 128 data points. Digital resolution in the final 3D spectrum was 7.52 Hz per point in F_3, 14.84 Hz per point in $F2$, and 15.63 Hz per point in F_1.

Pseudocontact shift calculations were performed using a set of Fortran programs developed by Emerson and LaMar (1990). The structure of the lipase-solubilized bovine cytochrome b_5 was used in these calculations (Mathews *et al*., 1979). Generally, in the calculation of susceptiblity tensors (Guiles *et al*., 1993, 1996) we have only used amide and α-carbon proton shift differences. Although we find that many side chain proton pseudocontact shifts are predicted accurately using these tensors, especially for many hydrophobic core residues, the accuracy is more limited for many side chain nuclei whose position is not nearly as accurately defined as are the backbone atoms.

Solution structures of both the wild-type rat ferrocytochrome b_5 and the A67V mutant in the region where chemical shift and NOESY peak intensity differences indicate that structural changes occur have been calculated using the program DIANA 2.1 (Güntert *et al.*, 1991). Structures were calculated for helix IV, the loop connecting helix IV to helix V, and helix V (i.e., residues 55 −71 and the heme). More

than 10 restraints per residue were used in these calculations (i.e., 11.8 restraints per residue for the wild type and 10.3 restraints per residue for the the A67V mutant). NOE peak intensity calibrations were performed using the program CALIBA (Güntert *et al.*, 1991). Only two restraints not directly derived from NOE or coupling constant data were included in the refinement. After several refinement cycles using redundant dihedral restraint procedures (i.e., REDAC refinement; Güntert *et al.*, 1991), it was apparent that the Nϵ nitrogen of H63 was the axial ligand to the iron (e.g., Fe−N distances ranged from 1.9 to 2.2 Å), and we included this as the restraint for both wild-type and mutant proteins. We also included a hydrogen bond restraint between the Nδ proton of H63 and the carbonyl oxygen of F58. In initial refinments this distance varied from 1.47 to 2.40 Å. This distance was restrained to 1.75 Å. NMR evidence for retention of this hydrogen bond in the A67V mutant is described in detail in Results.

The overall quality of the structures calculated can be ascribed to several factors. Unambiguous stereospecific assignments were obtainable for all prochiral protons except the β protons of S71 and the β and δ protons of R68 in the wild-type protein and the prochiral protons of S64, T65, S71, and R68 of the mutant due to a higher degree of amide degeneracies in the A67V mutant. Of the 201 restraints for the wild-type protein, 31 were long-range restraints, (including 21 restraints to the heme and 11 restraints to the imidazole ring of H63), 36 were mid-range restraints, 72 were sequential restraints, and 62 were intraresidue restraints. For the mutant protein, there were 35 long-range restraints (including 22 restraints to the heme and 13 restraints to the imidazole of H63), 28 mid-range restraints, 52 sequential restraints and 61 intraresidue restraints. For a full listing of restraints in DIANA 2.1 format, see Table S-1 in the Supporting Information.

We have only calculated the solution structure for the region of the protein encompassing domains involved in structural changes associated with the mutation (e.g., residues 55−71) for two reasons. First, there is an abundance of NMR experimental evidence that indicates that the solution structure of cytochrome b_5 strongly resembles the X-ray crystal structure, based on ring current calculations (Keller &Wüthrich, 1972; Guiles *et al.*, 1990), predictions of NOESY peak intensities based on complete relaxation matrix analyses (e.g., employing the program CORMA; Keepers & James, 1984) (Guiles *et al.*, 1990), and pseudocontact shift calculations (Veitch *et al.*, 1990, Guiles *et al.*, 1993). All of these calculations employed the crystal structure as a model for the solution structure. For the wild-type protein, the solution structure calculations presented here provide additional support to this assertion. Second, and more importantly, we needed evidence that solution structure methods were capable of demonstating statistically significant differences between mutant and wild-type proteins. For the specific question addressed in this study, that is, the reorientation of the imidazole ring induced by mutation, the answer is yes, with a statististical confidence of greater than 95% (e.g., angular rotation of the imidazole ring is more than two standard deviations away from the wild-type orientation; see Results for more details).

RESULTS

The approach to making ^{1}H, ^{15}N assignments of A67V rat cytochrome b_5 involved the following steps. Transfer of many amide proton resonances from the known assignments of wild-type rat ferrocytochrome b_5 to the mutant by superimposition of ^{15}N−proton heteronuclear correlation spectra was one step. These tentative assignments were confirmed through identification of spin systems in 2D DQFCOSY, HOHAHA, and 3D ^{15}N-filtered HOHAHA−HMQC spectra. Sequential connectivities were established through examination of 2D ^{1}H−^{1}H NOESY and 3D ^{15}N-filtered NOESY-HMQC spectra.

Assignment of resonances in the paramagnetic A67V rat ferricytochrome b_5 was accomplished by comparison of oxidized and reduced heteronuclear correlation spectra in an manner analogous to that described by Guiles *et al.* (1993). This procedure provided a set of tentative assignments. Sequential assignments were confirmed by examination of ^{15}N-edited NOESY−HMQC spectra. Spin system assignments were confirmed on the basis of 2D HOHAHA or HOHAHA-relayed HMQC spectra. Given this set of initial assignments, the orientation of the components of the magnetic susceptibility tensor could be calculated. Once known, predictions of chemical shift positions for various other residues could be made. Aided by these pseudocontact calculations, assignments of side chain resonances were made on the basis of systematic examination of cross-peak patterns in 500 MHz 3D NOESY−HMQC and HOHAHA spectra. Each of these steps is described in more detail below. More detailed descriptions of the assignment strategy for paramagnetic proteins using heteronuclear NMR methods are discussed by Guiles *et al.* (1993).

Transfer of Amide Proton Resonances from Rat Ferrocytochrome b_5 to A67V Ferrocytochrome b_5. Figure 1 contains an overlay of heteronuclear correlation spectra of rat cytochrome b_5 and rat A67V ferrocytochrome b_5. It is well-known that nitrogen-15 chemical shifts are most sensitive to changes in chemical structure (Kricheldorf, 1981). The vast majority of residues which show large changes in chemical shift are in the vicinity of the site of the mutation; e.g., of 13 amide resonances which shift by more than 0.1 ppm, 10 are within 6 Å of the site of mutation or the H63 imidazole (e.g., the β carbon of A67 or some heavy atom of the H63 imidazole ring). This is not surprising given a change from alanine to valine in a sterically limited space in the heme binding pocket. Some residues that are remote from the site of mutation, such ad W22, H26, and Y30 which lie in the β sheet, also show changes in resonance position.

The extent of heterogeneity observed in the mutant protein is similar to that in the wild-type protein. Once again nearly 40% of the resonances show doubling. Resonances that show resolved heterogeneity also show similar heterogeneity in the mutant. In the wild-type protein alanine 67 does not exhibit any observable heterogeneity. In the mutant, however, valine 67 clearly shows observable heterogeneity. There are no additional resonances that show heterogeneity nor is there a disappearance of heterogeneity for any of the other residues. In summary, comparison of heteronuclear correlation spectra gave us a set of plausible amide proton resonances for a large number of residues, which were ultimately confirmed by sequential methods.

Confirmation of Amide Assignment Transfer Using Sequential Connectivity Patterns. Using amide resonance assignments obtained from the previous step as a starting point, sequential connectivities were established by examination of 3D NOESY−HMQC spectra and 3D HOHAHA−HMQC spectra of reduced A67V rat cytochrome b_5. Homo-

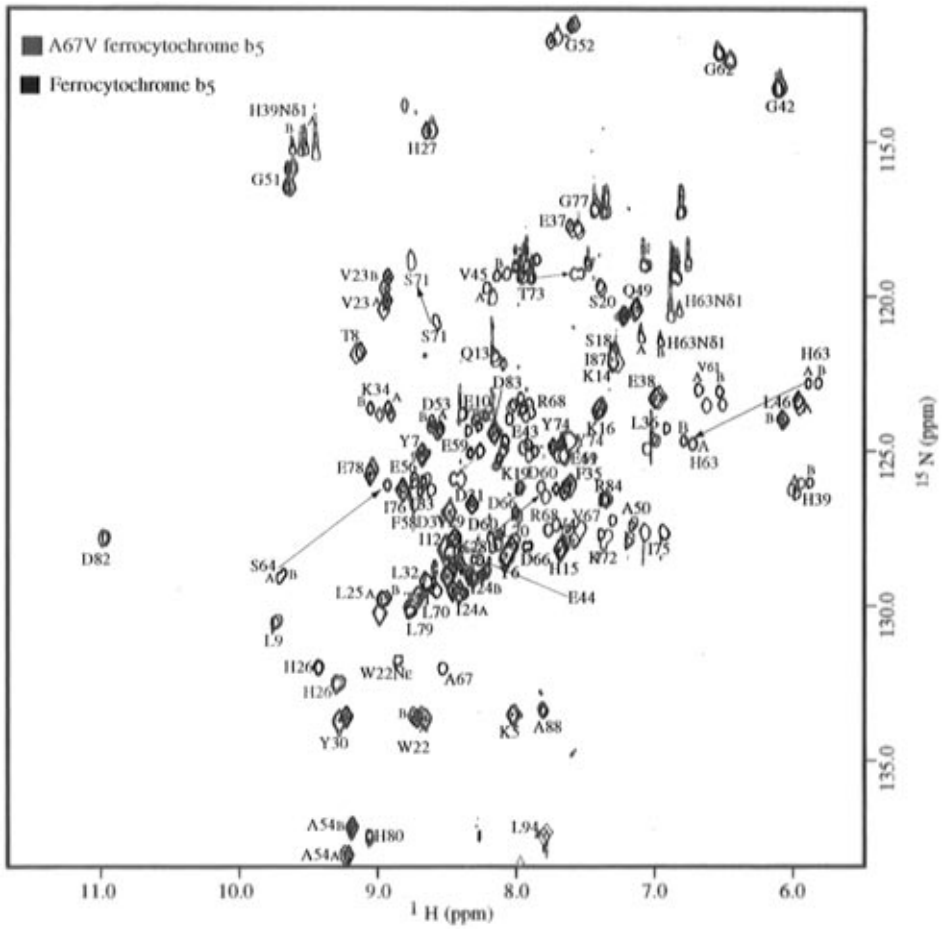

FIGURE 1: Overlay of 500 MHz $^{1}H-^{15}N$ heteronuclear correlation spectra of reduced wild-type and mutant proteins. Correlation peaks for ferrocytochrome b_5 are labeled with sequence-specific and conformation-specific resonance assignments. Arrows connecting the known assignments of the reduced wild type and those that are severely shifted in the mutant are shown for a few peaks in the vicinity of the mutation. Doubling of resonances for almost 40% of the residues is also observed for the mutant protein. Except for residues close to the site of mutation nearly all residues show clear overlap. The HMQC spectra shown were collected at 40 °C and a sample pH of 7.0.

nuclear $^{1}H-^{1}H$ NOESY, HOHAHA, and DQFCOSY were also used for identification of spin systems and for obtaining side chain to main chain connectivity information for aromatic residues. Assigned fingerprint peaks in the DQF-COSY are indicated in Figure S-1 in Supporting Information. As was observed in DQFCOSY spectra of the wild-type protein, a few Nα cross-peaks such as T33, H80, L36, and H39 are missing. This is probably due to the near-zero $^{3}J_{N\alpha}$ couplings. These resonances were observed in the 3D HOHAHA-HMQC spectra and NOESY spectra. The valine 67 side chain could be easily identified in the 2D $^{1}H-^{1}H$ HOHAHA and in the 2D $^{1}H-^{1}H$ NOESY. 3D NOESY−HMQC spectra show resolved resonances for most of the amide and side chain protons. Figure 2 shows sequential connectivities between residues 67 and 73 in the 3D NOESY−HMQC spectrum. These residues form a portion of helix V. Amide resonances of these residues show the largest changes in chemical shift position upon mutation.

There appear to be significant differences between wild-type and mutant proteins in the chemical shifts of some of the side chain protons, in particular for protons such as V61 γ methyls and H63 Hβ protons, all of which lie in the heme binding pocket. The origins of these shifts will be discussed later. (A complete listing of sequence-specific assignments for A67V ferrocytochrome b_5 is contained in Supporting Information, Table S- 2.) It is also striking that the resonances of the F58 side chain are clearly visible in the mutant protein but not in the wild-type protein (see Figure 3).

Isomer-Specific Assignments. Isomer-specific assignments were made solely on the basis of unique NOESY cross-peaks due to heme−proton to protein−proton connectivities which directly establish the specific orientation of the heme in the binding pocket. The pattern of isomer-specific assignments is identical to that found in the wild-type protein. As mentioned earlier, the only exception is the heterogeneity detectable for valine 67. The γ methyls of V67 show direct contacts to heme proton resonances; hence they could be easily assigned. The amide proton resonances show near alignment but are well separated in chemical shift at the α, β, and γ protons for both isomers.

Heme Proton Resonance Assignments. Assignments for heme resonances (Table 1) in the mutant protein show that there are differences in chemical shift positions for almost all heme resonances. However, examination of 2D $^{1}H-^{1}H$ NOESY spectra does not show connectivities to the heme from residues other than those observed in the wild-type protein, and normalized amplitudes of those NOE cross-peaks are similar to those of the wild-type proteins. Thus, we have not found any evidence for a change in the orientation of the heme in both equilibrium forms from that found in the wild-type protein (Pochapsky *et al.*, 1990., Guiles *et al.*, 1992). Furthermore, the striking similarity in resonance

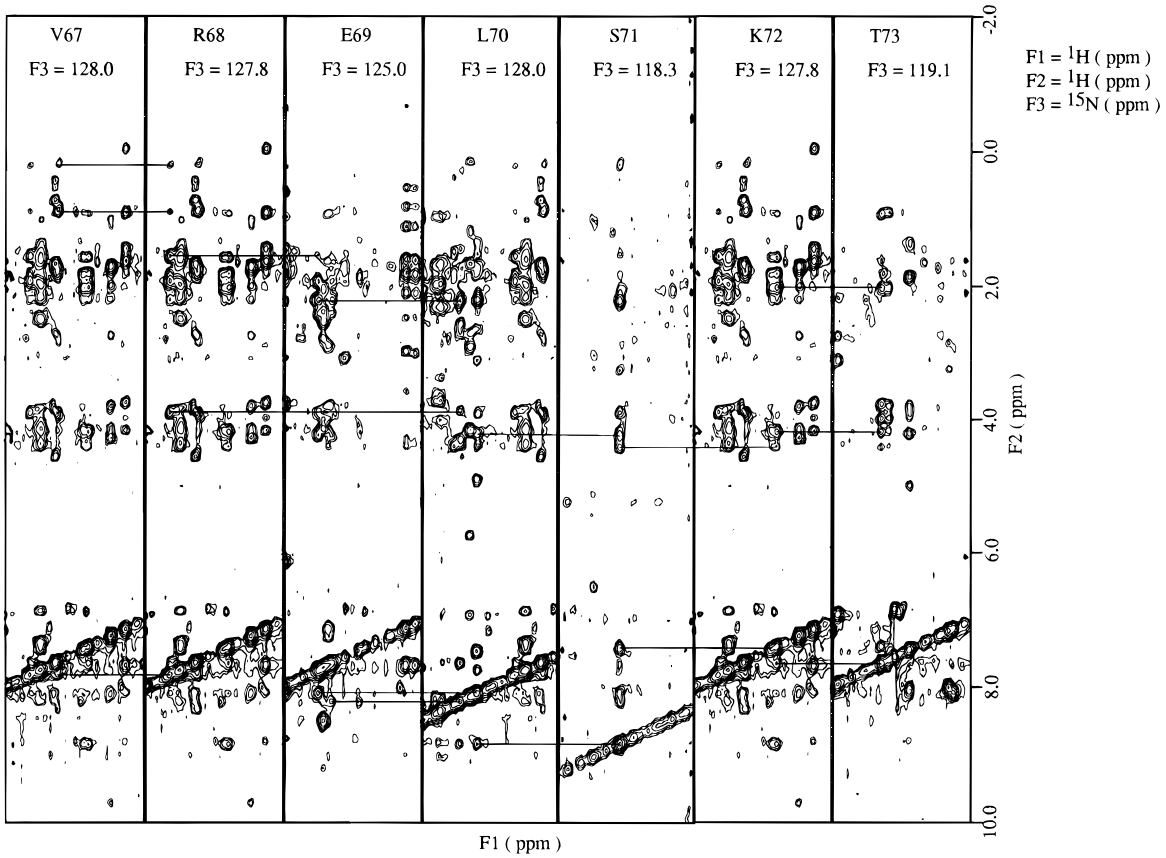

FIGURE 2: Strip plot of a 3D ^{15}N-filtered NOESY−HMQC spectrum of rat ferricytochrome b_5 showing sequential connectivities between residues 67 and 73 which are the central residues in helix V. These residues show the largest changes in chemical shift positions for the amide protons on mutation. Due to alignment in the amide proton resonance positions of R68 and E69, the NH_i-NH_{i+1} correlation peak, which is characteristic in helical regions, is not observed. The remaining residues show strong NH_i-NH_{i+1} correlation peaks that assisted in making sequential assignments.

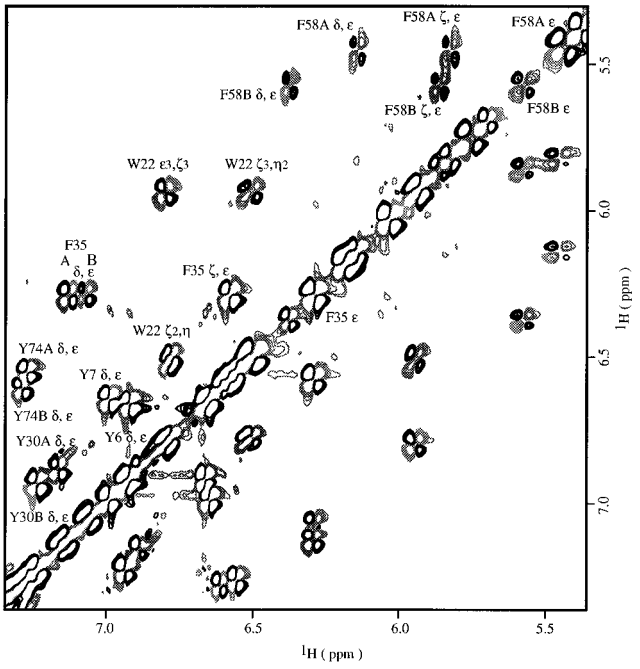

FIGURE 3: Contour plots of the aromatic region of A67V rat ferrocytochrome b_5. The appearance of correlation peaks for the F58 ring in both equilibrium forms is indicative of an alteration in the motional characteristics of the F58 ring. These resonances were not seen in the wild-type protein.

positions of nuclei remote from the site of mutation argues strongly against heme reorientation.

Structural Perturbations on Mutation Are Minimal. An overlay of heteronuclear correlation spectra of the wild-type and mutant proteins in the reduced form (Figure 1) shows that most of the resonances overlay very well. The only exceptions are a short stretch of residues on either side of the mutation that show changes in both amide ^{15}N and amide proton chemical shift positions. Of 86 assigned amides in HMQC spectra of wild-type and mutant proteins, 57 lie within 0.05 ppm, 15 lie within 0.1 ppm and 14 differ by greater 0.1 ppm. While it is well-known that changes in chemical shift are difficult to correlate with changes in structure, the pattern of intraresidue NOESY connectivities and NOESY connectivities between side chain protons of

Table 1: Heme Proton Resonance Assignments[a] of Reduced WT and A67V Cytochrome b_5

	A67V		WT	
assignment	isomer A	isomer B	isomer A	isomer B
α-meso	9.38	9.57	9.29	9.48
β-meso	9.84	9.91	9.79	9.77
γ-meso	9.46	9.43	9.32	9.34
δ-meso	9.96	9.80	9.89	9.76
2-HC_α	7.43	7.97	7.41	7.87
2-HC_β (trans)	5.38	6.19	5.42	6.23
2-HC_β (cis)	5.08	5.70	5.06	5.69
4-HC_α	8.29	8.04	8.27	8.34
4-HC_β (trans)	6.03	5.14	6.05	5.48
4-HC_β (cis)	5.92	5.27	5.96	5.19
1-CH_3	3.29	3.55	3.28	3.52
3-CH_3	3.43	2.97	3.38	2.87
5-CH_3	3.56	3.70	3.52	3.64
8-CH_3	3.74	3.51	3.66	3.54

[a] All spectra on which these assignments are based, e.g., DQFCOSY, HOHAHA, and NOESY, were recorded at 40 °C, pH 7.0, in 100 mM phosphate buffer. Heme protons are designated according to the nomenclature used by Pochapsky *et al.* (1990).

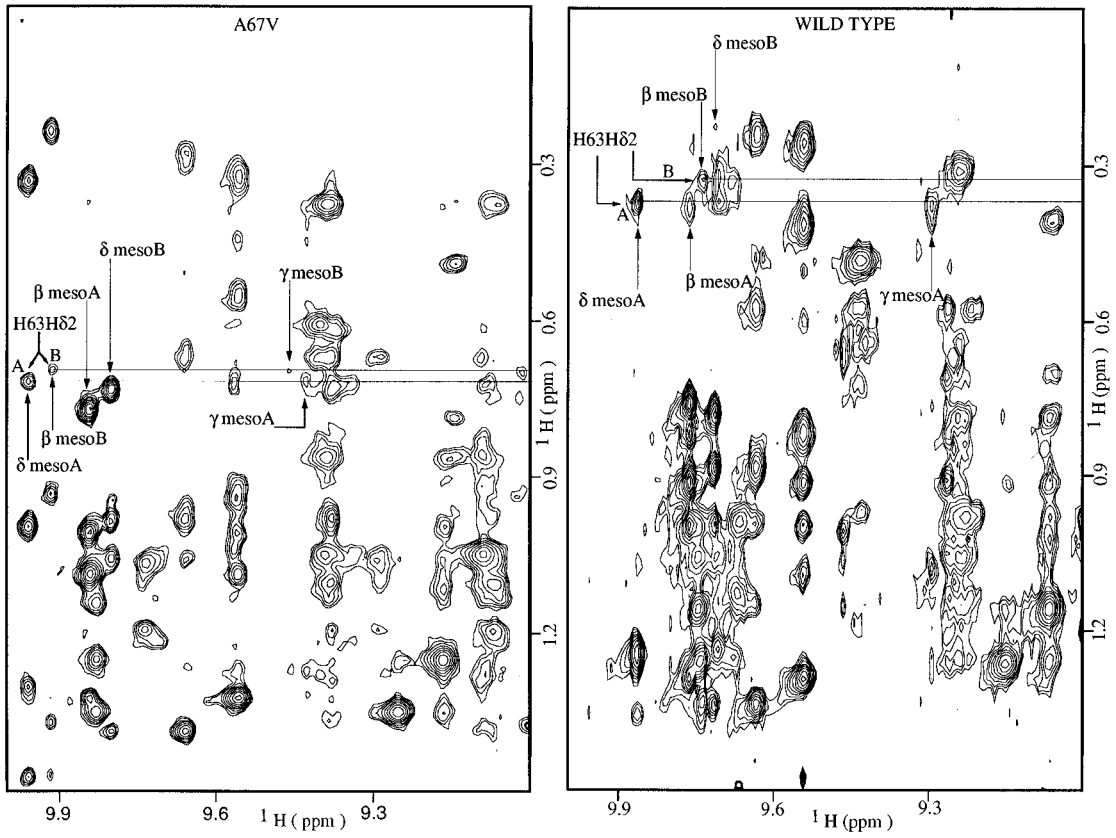

FIGURE 4: Contour plots of the 600 MHz 2D ^{1}H$-^1$H NOESY spectrum showing connectivities between the H63Hδ2 proton and the γ meso proton in the mutant rat ferrocytochrome b_5 protein. The corresponding correlation peak is absent in the spectrum of the wild-type protein.

residues that line the heme binding pocket and heme is almost identical, indicating that there is very little displacement of these side chains.

Due to the steric perturbations caused by a mutation from alanine to valine, it was of concern to us whether the H63 ring had reoriented in a manner to disrupt the hydrogen bond between H63Nδ1H and the backbone carbonyl of F58 residue. We have evidence that the hydrogen bond is intact. The 3D ^{15}N-filtered NOESY$-$HMQC spectra show NOE connectivities of comparable intensity between F58Hα and H63Nδ1H protons for both wild-type and mutant proteins (see Figure S-3 in Supporting Information). This suggests, at a minimum, that the H63 Nδ proton remains in close proximity to the backbone in the region of F58. Also it is important to point out that neither ^{15}N nor proton resonance positions of the Nδ atom of histidine 63 shift significantly relative to the wild type. Previous ^{15}N NMR studies of histidine side chains showed conclusively that ^{15}N resonances are particularly sensitive to hydrogen-bonding effects. Shifts in ^{15}N resonance position upon breaking a Nδ1 hydrogen bond have been observed to be $\sim$10 ppm (Smith *et al.*, 1989). Other connectivities to the ring suggest that there is a reorientation of the H63 ring in the mutant. Most notable are the NOESY connectivities from the H63Hδ2 proton to the γ meso heme proton (Figure 4) and from the H63Hϵ1 to the 4HCβ (trans) proton. These connectivities are not observed in the wild-type protein. In the wild-type protein, the H63Hϵ1 proton shows connectivities to both the 8-CH_3 and 1-CH_3 protons in the B-form while in the mutant only the cross-peak to the 1-CH_3 proton is observed. Also, the H63Hδ2 proton shows connectivities to both the 1- and 8-methyl protons of the heme in the wild-type protein while it shows connectivities to only 8-methyl protons in the mutant

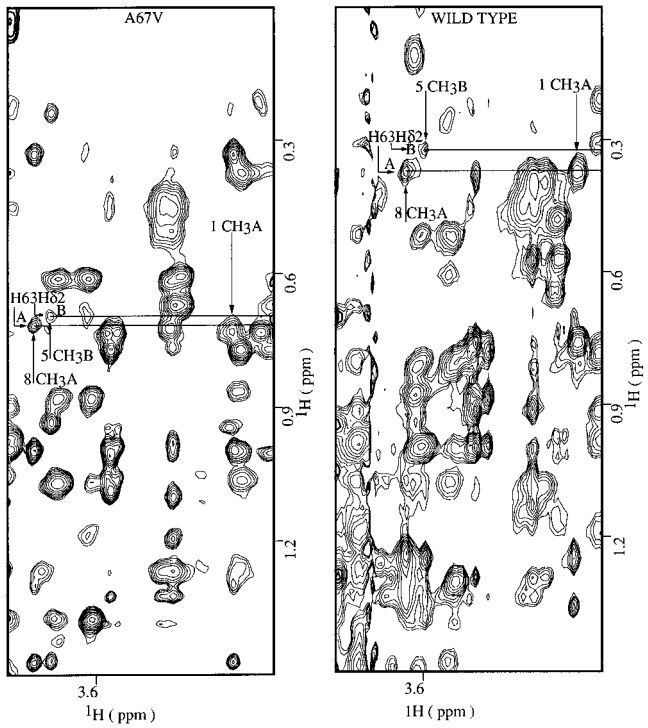

FIGURE 5: Contour plots of the 600 MHz 2D ^{1}H$-^1$H NOESY spectra of mutant (A) and wild-type (B) rat ferrocytochrome b_5 proteins showing connectivities between H63Hδ2 and heme methyl protons. The absence of a correlation peak between H63Hδ2 and the 8-methyl protons in the A conformer in the mutant, when taken in conjunction with the results shown in Figure 8, is indicative of a reorientation of the H63 axial ligand.

protein (Figure 5). The detailed solution structure calculations described below indicated a statistically significant reorientation of the H63 imidazole consistent with these

Table 2: Precision of the Structures of the Domains of Wild-Type Rat Cytochrome b_5 and the A67V Mutant[a]

	wild type		A67V	
residues	av local rmsd (backbone)	av local rmsd (heavy atom)	av local rmsd (backbone)	av local rmsd (heavy atom)
all (55−71)	0.30 ± 0.20	1.25 ± 0.47	0.38 ± 0.19	1.37 ± 0.39
helix IV (55−71)	0.28 ± 0.23	1.36 ± 0.48	0.32 ± 0.21	1.12 ± 0.21
strand I (62−65)	0.26 ± 0.10	0.73 ± 0.48	0.49 ± 0.21	1.31 ± 0.55
helix V (66−71)	0.37 ± 0.23	1.41 ± 0.27	1.41 ± 0.14	1.72 ± 0.12

[a] Local rmsd calculations tabulated here represent a running three-residue superposition of atoms for the 20 structures with the lowest target function value.

FIGURE 6: Stereo representation of the 20 refined solution structures of wild-type rat ferrocytochrome b_5 in the region containing residues 55−71 and the heme. The plots display the backbone atoms and side chains for a number of well defined residues in the hydrophobic heme binding pocket. Shown are the V61 side chain on the left-hand side of the image, the H63 side chain containing the axial imidazole, and the A67 side chain on the right-hand side of the image. Helix IV is on the right-hand side of the stereo image, and helix V is on the left hand side. For clarity only one of the hemes is shown in the figure.

FIGURE 7: Stereo representation of the 20 refined solution structures of the A67V mutation of rat ferrocytochrome b_5 in the region containing residues 55−71. The plots display the backbone atoms and side chains for a number of well-defined residues in the hydrophobic heme binding pocket. Shown are the V61 side chain on the left-hand side of the image, the H63 side chain containing the axial imidazole, and the V67 side chain on the right-hand side of the image. Helix IV is on the right-hand side, and helix V is on the left-hand side. For clarity only one of the hemes is shown in the figure. The orientation is similar to that shown for the wild-type protein.

observations. However, it is important to note that the rmsd variation in atom positions in the mutant protein is significantly greater than that of the wild type despite a comparable number of restraints. Possible origins of these differences are discussed below.

Analysis of the Calculated Solution Structures: Differences Induced by Mutation. Four cycles of iterative structure refinement followed by NMR restraint verification and distance restraint refinement were performed. In each cycle 200 structures were generated and subjected to three cycles of redundant dihedral angle restraint refinement, and the 20 structures with the lowest target function values were retained for statistical analysis. Table 2 contains a summary of statistical data indicating the quality of the structures generated for both wild-type and mutant proteins. As can be seen from a comparison of Figures 6 and 7, the global folds of the wild-type protein and the A67V mutant protein are remarkably similar. Note that the rmsd variation in the backbone of the mutant protein is significantly greater than that of the wild-type protein. We do not believe that this is due to the slightly lesser number of restraints in the mutant protein. In fact, the number of long-range restraints is greater in the mutant protein than it is in the wild type. This is largely due to restraints to the F58 ring. Resonances of the F58 ring were observable in the mutant but not in the wild-type protein. As described below, the dynamics of side chains in the hydrophobic heme binding pocket have no doubt been altered in the mutant protein. As a result of the lack of restraints in the wild-type protein, the orientation of the F58 ring is not well defined in the wild-type solution structure; however, in the solution structure of the mutant protein the angular orientation of the F58 is restrained due to the existence of four NOE restraints to this ring system. The apparent stacking of the F58 ring on the H63 ring in the solution structure of the mutant is similar to that observed in the bovine protein crystal structure.

The orientation of the imidazole side chain of the axial histidine is remarkably well-defined in both the mutant and wild-type proteins. Presumably this is due to the large number of restraints to this ring in both proteins (e.g., 11 restraints to the ring in the wild type and 13 in the mutant). The number of restraints for this residue is also anomalously large (e.g., there are 30 restraints to H63 in the wild type and 23 restraints in the mutant). An overlay of the imidazole rings from the 20 refined structures for both the wild-type and mutant proteins is shown in Figure 8 relative to the heme

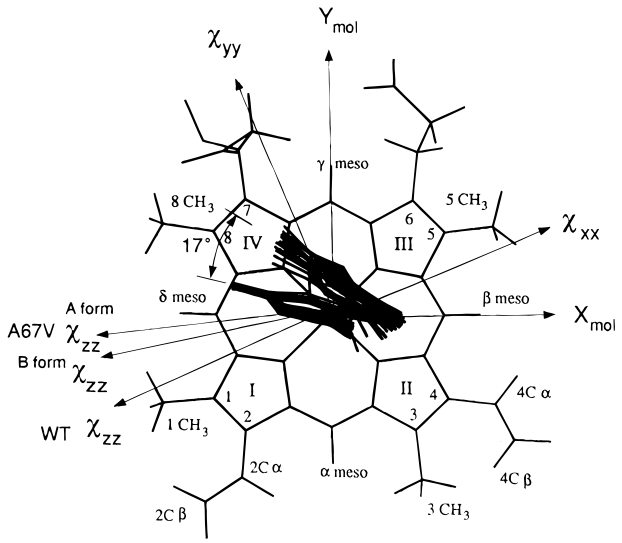

FIGURE 8: View of the heme which indicates the reorientation of the axial imidazole induced by the A67V mutation. Imidazoles from all 20 solution structures of rat ferrocytochrome b_5 and the A67V mutation are shown. Imidazole structures are shown relative to a single fixed heme orientation which is shown. Average angular displacement of the imidazole of 17° is shown. The orientation is of the in-plane components of the magnetic susceptibility (χ_{xx} and χ_{yy}) and a projection of the axial component (χ_{zz}) onto the *x*, *y* plane. The direction of rotation of the *z*-component of the magnetic axis is in the direction of rotation of the H63 ring and is equal in magnitude. The heme nomenclature used in the text is indicated on the figure.

which is fixed for all 40 structures shown. Given the range of variation in the angular orientation of the imidazole rings, its is possible to define limits on the uncertainty in the rotation of the imidazole plane. The imidazole of the mutant protein has rotated in a counterclockwise direction (i.e., viewing the heme iron from the H63 face as shown) by 17 ± 7° relative to the wild-type imidazole orientation. The majority of the uncertainty in the angular reorientation of the H63 imidazole ring arises from the scatter observed in the orientation in the mutant protein. It is also important to note that the orientation of the imidazole ring in the wild-type solution structure is virtually identical to that of the bovine X-ray crystal structure.

The V61 methyls and the methyl of A67 flanking the H63 imidazole are positioned in a similar manner to the methyls of V61 and the V67 γ' methyl in the mutant protein (see Figures 3 and 4). In fact, the pairwise rmsd variation in the position of the methyl of A67 relative to the position of the V67 γ' methyl in overlays of the structure of the mutant on that of the wild type where the heme is held in a fixed orientation is only 0.63 Å. However, the greater steric bulk of the valine in the mutant forces a slight reorientation of helix V and the loop connecting helix VI and helix V. This accounts for some of the differences in the orientation of the H63 imidazole. It is also consistent with observed chemical shift changes in this region of helix V.

Ranges of elements of secondary structure calculated for the solution structure of the wild-type protein are similar to those of the X-ray crystal structure. Helix IV is very well-defined in the solution structure and ranges from T55 to V61 as it does in the crystal structure. The loop ranging from G62 to T65 is also superimposable on the crystal structure within the rmsd of the backbone atoms. However, only a single turn of helix V is well-defined in the wild-type solution structure ranging from D66 to E69. In the crystal structure this helix extends from D66 to S71. Fraying of the end of this helix may be due to a more limited range of restraints in this region of the structure. In the mutant solution structure the range of helix V more closely resembles that of the X-ray crystal structure. Midrange restraints defining this helical domain were more complete for the mutant than they were for the wild-type protein.

Calculation of the Orientation of the Susceptibility Tensor. The methodology for transfer of assignments from a diamagnetic protein to an isostructural paramagnetic protein containing a single rapidly relaxing nonisotropic paramagnetic center using $^{15}N-^{1}H$ heteronuclear methods has been fully described by Guiles *et al.* (1993). Briefly, overlays of oxidized and reduced $^{15}N-$proton heteronuclear correlation spectra allow for transfer of many amide proton resonances that are not severely shifted by the dipolar field. Figure 9 shows an overlay of oxidized and reduced A67V rat cytochrome b_5. For many nuclei that are located in the diamagnetic regions of the protein remote from the heme or at zero crossing points for the dipolar field, the magnitude of the shifts are small. For a number of residues, e.g., D82, L9, K5, D83, and R84, the peaks are nearly superimposable.

Confirmation of Amide Assignment Transfer Using Sequential Connectivity Patterns. Using the amide proton resonance assignments in the previous step as a starting point, sequential connectivities were established through examination of 3D NOESY−HMQC spectra of oxidized A67V rat cytochrome b_5. Once a sufficient number of amide proton resonances had been assigned by standard sequential methodologies, it was possible to calculate the orientation of the paramagnetic tensor, as described in the next section. In this manner sequential connectivities seen in the 3D NOESY−HMQC helped to confirm the amide assignments transferred using the overlay of heteronuclear correlation spectra.

Calculations of the Susceptibility Tensor. We used an iterative process to complete the assignments. Once a sufficient number of assignments were available for both the oxidized and reduced forms of A67V rat cytochrome b_5, it was possible to calculate the orientation of the susceptibility tensor for the unknown anisotropic paramagnetic tensor using the bovine crystal structure as a model for the mutant A67V rat cytochrome b_5. Starting point magnitudes of the components of the anisotropic susceptibility were estimated using low-temperature EPR spectra (Weissbluth, 1967). Tensor calculations were performed on the basis of amide assignments in both states. Once the tensor orientation was known, predictions for all other resonances of the paramagnetic protein could be made. These predictions were used to guide assignments of resonances more severely shifted. With progressive assignments, more accurate susceptibility tensors could be calculated. This process was repeated until a nearly complete set of resonance assignments were obtained.

Table 3 contains the susceptibility tensor parameters for the two different conformations of the heme obtained using this set of data. Figure 10 shows linear regression plots of calculated versus observed shifts for both final optimized tensor orientations. Regression parameters are shown for the set of data displayed. Large deviations occur from the linear relationship for certain residues. Similar deviations were also found in the tensor analysis for the wild-type protein; the reasons for these deviations have been described earlier (Veitch *et al.*, 1990; Guiles *et al.*, 1993). Calculation of the orientation of the susceptibility tensor from the observed dipolar shifts shows that the angular orientations

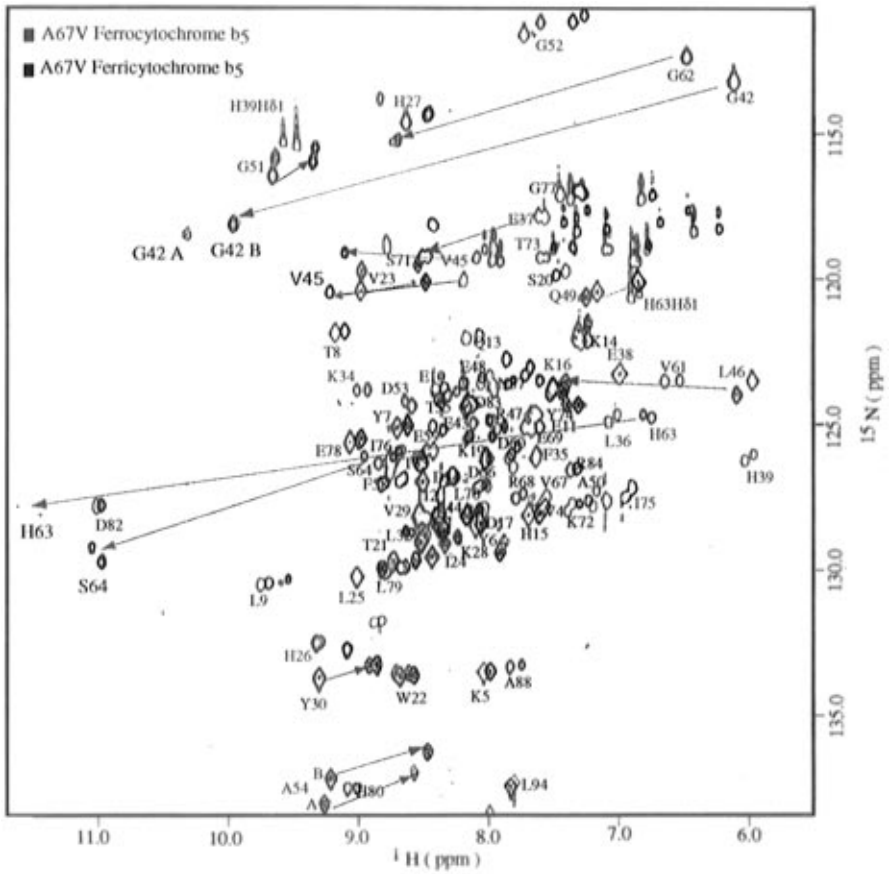

FIGURE 9: Overlay of a contour plot of a $^1H-^{15}N$ heteronuclear correlation spectrum of A67V rat ferricytochrome b_5 on that of A67V rat ferrocytochrome b_5. Arrows connecting the known assignments of the reduced protein to the corresponding heteronuclear correlation peaks in the paramagnetic protein are shown for a few peaks.

Table 3: Components of the Susceptibility Tensor for Equilibrium Conformations of Wild-Type and Mutant Proteins[a]

	A67V		wild type	
	A	B	A	B
$\Delta\chi_{ax}$	1643×10^{-12}		1643×10^{-12}	
$\Delta\chi_{rh}$	-847×10^{-12}		-847×10^{-12}	
α	6	12	23	25
β	9	9	8	9
γ	17	17	0	4
in-plane rotation $\alpha + \gamma$	23	29	23	29

[a] Axial and rhombic components of the anisotropic susceptibility and Euler angles are defined as described by Emerson and La Mar (1990). Susceptibilities are expressed in Van Vleck units (m^3/mol) as described by Horrocks and Hall (1971). Euler angles are expressed in degrees. Uncertainties in Euler angles are ±6°, based on the point at which the least squares residual in the fit to the observed shifts doubles, all other variables being held constant.

of the in-plane components of the mutant protein are identical with those of the wild-type protein. However, there are significant differences in the individual components of the tensor. Figure 8 shows the orientation of the magnetic axes for both equilibrium forms of the mutant and wild-type proteins. Also displayed are the orientations of the imidazoles for the A-forms of the proteins determined from the solution structure analyses for both the wild-type and mutant proteins. Note that both the magnitude and direction of rotation of the imidazole plane and the *z*-component of the susceptiblity tensor are remarkably similar. The *z*-component of the susceptiblity tensor was reoriented 17 ± 6° relative to the wild-type, and the imidazole plane has also rotated 17 ± 7° in the same direction.

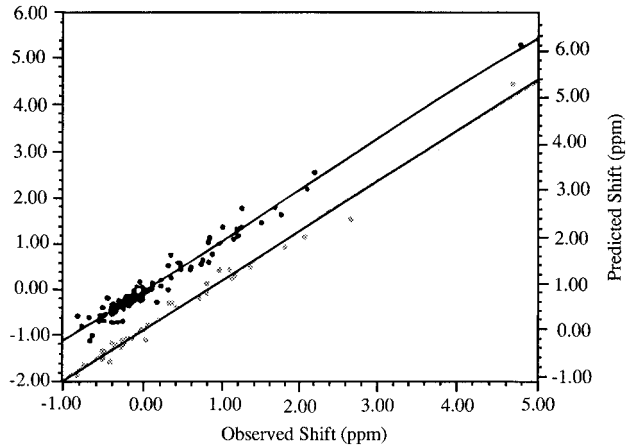

FIGURE 10: Linear regression plots of calculated versus observed dipolar shifts for the amide and C_α protons of the A-form of A67V rat ferricytochrome b_5 (points shown offset in black) and amide protons of the B-form (points shown in gray offset below the A-form plot). The vertical scale on the left-hand side of the plot refers to the A-form data while the vertical scale on the right references the B-form data. The regression parameters for the least squares fit to the 145 points plotted for the A-form are slope = 1.12, intercept = 0.03, and $R^2 = 0.966$. The regression parameters for the least squares fit to the 41 points plotted for the B-form are slope = 1.11, intercept = −0.01, and $R^2 = 0.985$. Only amide protons which differed by more than 0.02 ppm between the two different conformations are plotted for the B-form data. Calculated values in each case are based on the susceptibility parameters contained in Table 3.

DISCUSSION

Mutant Design Philosophy. Our objective was to produce as minor a structural modification of the whole protein as

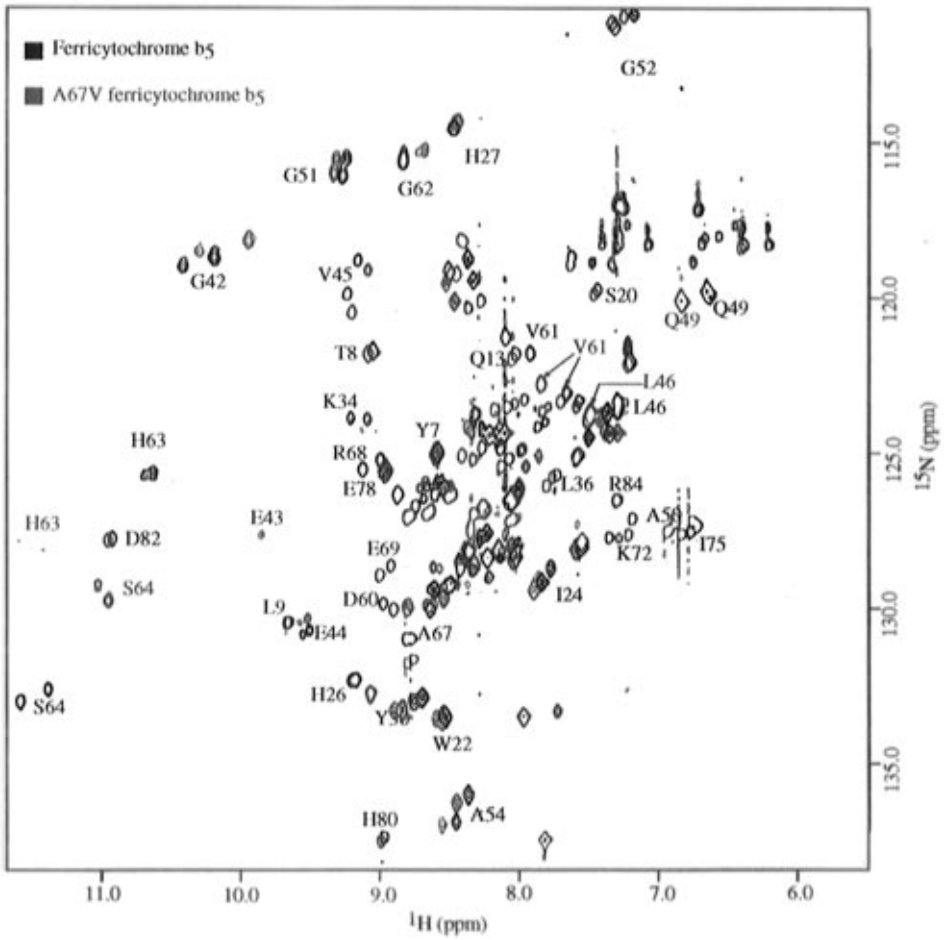

FIGURE 11: Overlay of a contour plot of a $^1H-^{15}N$ heteronuclear correlation spectrum of ferricytochrome b_5 on that of A67V ferricytochrome b_5. Reorientation of the axial component of the magnetic susceptibility tensor is manifested by differences in shift positions of a number of residues. Certain residues that are perfectly superimposable in the reduced form, e.g., L46, Q49, A50, and V45, exhibit such shifts. Residues in the diamagnetic region of the proteins such as T8, L9, H80, and D82 are nearly perfectly superimposable. The HMQC spectrum was recorded at 600 MHz, at 40 °C, and with a sample pH of 7.0.

possible and achieve reorientation of individual axial imidazole ligands. The A67V mutation achieved this goal through the substitution of a bulkier, hydrophobic ligand for a residue in the hydrophobic binding pocket in contact with the H63 imidazole ring. Initially we believed this would result in a disruption of a hydrogen bond between the H63Nδ proton and the main chain carbonyl of residue 58. Contrary to our initial expectations, structural changes induced by mutation achieved reorientation of the imidazole ring without breaking this hydrogen bond, as described below.

Structural Changes. The overall global fold of this domain of the protein is largely maintained (compare Figures 6 and 7). Also, the positions of many side chains in the hydrophobic pocket are also largely unperturbed upon mutation. The positions of the γ methyls of V61 are remarkably similar in both mutant and wild-type proteins. Similarly, although the orientation of the F58 phenyl ring is not well defined in the wild-type protein (i.e., due to a complete lack of restraints), the orientation of this ring in the mutant is similar to that observed in the crystal structure (i.e., stacked against the H63 imidazole). As noted earlier, the positions of the β methyl of A67 and the γ' methyl of V67 are also remarkably similar, within the resolution of the structures. As indicated by a detailed comparison of the solution structures of the mutant and wild-type proteins (see Figure 8), the reorientation of the H63 imidazole ring is not a simple twist about the iron imidazole nitrogen bond but involves a slightly more complex gyration involving a twist coupled with a slight displacement of the ring away from the Fe center.

The bulkier side chain of V67 forced a slight displacement of helix V away from the heme in the vicinity of the mutation. A slight twist of the loop connecting helix IV and helix V toward the heme iron was also induced. The net effect of these distortions was a slight expansion of the heme pocket. Further support for this assertion comes from the observed increase in side chain dynamics for residues in the heme binding pocket. In studies of mutant myoglobins it has been found that replacement of histidine with a glycine or valine results in a contraction of the heme binding pocket (Rajarathnam *et al.*, 1993).

Correlations between Structural Changes and Observed Chemical Shift Changes. Chemical shift changes are often taken as an indication of structural changes (Gao *et al.*, 1991) occurring in a protein structure as the result of mutation or the binding of a ligand (Shuker *et al.*, 1996). Although it is difficult to correlate changes in chemical shift with exact changes in structure, near identity of chemical shifts can indicate structural similarity, especially when analyzed in conjunction with NOE data. Except for residues neighboring the region of mutation, almost all other heteronuclear cross-peaks (see Figure 1) show remarkable superimposability (e.g., K5, L9, H15, S20, F35, Q49, G77, H80). Examination of NOE data for both wild-type and mutant proteins shows remarkably similar short- and long-range NOE connectivities.

This is particularly so on the H39 side of the heme. Thus the small chemical shift changes and the NOE connectivities indicate that reorientation of the H39 imidazole ring is negligible. On the other hand, regions of the protein where the solution structure calculations indicate that significant structural changes did occur are reasonably well-defined by significant shifts in heteronuclear correlation peaks (see Figure 1). Certain residues in the heme binding pocket and in strands 3 and 4 of the β sheet [see Mathews *et al*. (1979) for nomenclature] show small shifts (e.g., less than 0.1 ppm) in amide resonance positions (e.g. W22, L25, Y30). This could be the effect of a further small realignment of the axial imidazole planes with respect to each other.

Altered Dynamics in the Heme Binding Pocket and Orientation of the H63 Ring. One of the most surprising effects of the mutation has been the change in rate of rotation of the F58 ring. In the crystal structure of bovine cytochrome b_5 the rings of H63 and F58 are stacked against one another (Mathews *et al.*, 1979). The observed proton NMR resonances for the F58 ring of the A67V mutant are conformationally averaged, and thus it is safe to assume that the rate of ring rotation has increased. The other aromatic residue in the heme binding core (e.g., F35) does not show any change in its dynamic properties. The increased rate of rotation of the F58 ring is probably the result of a slight expansion of the heme pocket coupled to the imidazole reorientation. Any expansion of the heme pocket would occur on the side of the mutation, i.e., a movement of helix V away from the iron center. NOE contacts observed between S71NH and S71Hα to 1-methyl and 3-methyl protons of the heme in the A- and B-forms, respectively, argue against a movement of the entire helix but only of residues in the immediate vicinity of the mutation as is observed in the solution structure calculations.

A slight distortion of helix V and the reorientation of the H63 are probably not the only changes resulting in the increase in rate of the F58 ring rotation. The rmsd variation in the backbone of the mutant protein was observed to be somewhat greater than that of the wild-type protein despite a greater number of long-range restraints used in the refinement of the solution structure of the mutant. We believe the lower precision in the placement of the backbone atoms may reflect, in part, some of the enhanced dynamics of the binding pocket of the heme on the H63 face of the heme, indicated by the increased mobilitiy of the F58 ring in the mutant.

Reorientation of the Paramagnetic Susceptibility Tensor. Factors dictating the reorientation of the paramagnetic susceptibility tensor are less clear for cytochrome b_5 than for other systems such as cytochrome *c* and myoglobin. The orientation of the *z*-axis in both cytochrome *c* and myoglobin is dominated by a single short axial bond whereas the presence of bis(histidine) axial ligands in cytochrome b_5 precludes a model based on the dominance of one ligand over the other. It has been suggested that the His-39−Fe bond determines the in-plane magnetic axes (Lee *et al.*, 1993). The reorientation of the H63 imidazole in A67V cytochrome b_5 has no observable effect on the orientation of rhombic components of the magnetic susceptibility tensor. The in-plane tensor components appear to track the orientation of the heme in the two forms which, based on the patterns of NOESY connectivities, is identical to the wild-type protein. There are, however, significant differences in the orientations of the individual components of the tensor. For instance, the Euler angles defining the orientation of the in-plane components for the mutant are 6° (α) and 17° (γ) for the A-form and 12° (α) and 17° (γ) for the B-form, quite different individually from the wild-type values. Thus, the reorientation of the susceptibility tensor in A67V cytochrome b_5 is a sensitive probe for local structural changes.

Differences in the α angles indicate that the *z*-component of the susceptibility tensor of the A67V mutant has rotated an additional 17° for the A-form and 13° for the B-form, toward the δ meso proton relative to the wild-type protein. The rotation of the *z*-component of the tensor is in the same direction of rotation of the axial ligand (H63). Also the magnitude of the rotation of the *z*-component of the susceptibility tensor is similar to the magnitude of the rotation of the imidazole ring (e.g., both have mean magnitudes of 17°). The sensitivity of nuclei to pseudocontact shifts is determined by their position relative to the paramagnetic center. Examination of the relative axial and rhombic contributions to the predicted pseudocontact shifts shows that there is a greater positive axial contribution for the shifts of L46 and R47 amide protons and a less negative axial contribution to the shifts of E48, Q49, and A50 amide protons in the A67V mutant relative to the wild-type protein. At the same time the axial contribution to the predicted shifts of F58 is more negative and those for E59, D60, and V61 are less positive. These residues all lie in the two octants that are bordered by the α and β meso protons, above and below the plane of the heme. The observed shifts of these residues are consistent with the predicted shifts and the direction of tilt of the *z*-component of the magnetic susceptibility tensor. Qualitatively, the reorientation of the susceptibility is clear from a comparison of Figures 1 and 11 which show that in the reduced proteins correlation peaks associated with L46, Q49, and A50 are perfectly superimposable, whereas they are not in the oxidized proteins. Similar reorientation of the susceptibility tensor has been observed for distal point mutants of cyanometmyoglobin (Rajarathnam *et al.*, 1992). Changes in the orientation of the susceptibility tensor also are indicative of changes in the electronic structure of the iron which can be correlated with observed changes in EPR, optical, and electrochemical properties of the system which are discussed in more detail in the accompanying paper.

ACKNOWLEDGMENT

We thank Dr. Steven Sligar for the kind gift of the plasmid encoding the soluble heme binding domain of rat cytochrome b_5. We also thank Dr. Michael Summers for the use of the 600 MHz NMR spectrometer at the University of Maryland Baltimore County and Zeneca Pharmaceuticals for allowing use of their Bruker 500 MHz AMX NMR spectrometer.

SUPPORTING INFORMATION AVAILABLE

Three tables containing complete restraint sets used in the solution structure calculations in DIANA 2.1 format (Table S-1) and proton and nitrogen-15 assignments for rat A67V ferrocytochrome b_5 (Table S-2) and rat ferricytochrome b_5 (Table S-3) and three figures containing fingerprint peak assignments of the DQFCOSY spectrum of A67V rat ferrocytochrome b_5 (Figure S-1), strip plots from the NOESY spectrum of the mutant protein indicating V67 to heme and protein connectivities (Figure S-2), and strip plots from 3D NOESY HSQC spectra of mutant and wild-type proteins

indicating H63 imidazole to F58Hα connectivities (Figure S-3) (24 pages). Ordering information is given on any current masthead page.

REFERENCES

Bax, A., & Davis, D. G. (1985) *J. Magn. Reson. 65*, 355−360.
Bax, A., & Grzesiek, S. (1993) *Acc. Chem. Res. 26*, 131−138.
Bax, A., Griffey, R. H., & Hawkins, B. L. (1983) *J. Magn. Reson. 55*, 301−315.
Clore, G. M., & Gronenborn, A. M. (1991) *Prog. Nucl. Magn. Reson. Spectrosc. 23*, 43−92.
Cutler, R. L., Davies, A. M., Creighton, S., Warshel, A., Moore, G. R., Smith, M. & Mauk, A. G., (1989) *Biochemistry 28*, 3188−3197.
Emerson, S. D., & La Mar, G. N. (1990) *Biochemistry 29*, 1545−1556.
Feng, Y., Roder, H., & Englander, S. W. (1990) *Biochemistry 29*, 3494−3504.
Gao, Y., Veitch, N. C., & Williams, R. J. P. (1991) *J. Biomol. NMR 1*, 457−471.
Gochin, M., & Roder, H. (1995) *Protein Sci. 4*, 296−305.
Griesinger, C., Otting, G., Wüthrich, K., & Ernst, R. R. (1988) *J. Am. Chem. Soc. 110*, 7870−7872.
Guengerich, F. P., Ed. (1987) *Mammalian cytochromes P-450*, Vols. 1 and 2, CRC Press, Boca Raton, FL.
Guiles, R. D., Altman, J., Lipka, J. J., Kuntz, I. D., & Waskell, L. (1990) *Biochemistry 29*, 1276−1289.
Guiles, R. D., Basus, V. J., Kuntz, I. D., & Waskell, L. (1992) *Biochemistry 31*, 11365−11375.
Guiles, R. D., Basus, V. J., Sarma, S., Malpure, S., Fox, K. M., Kuntz, I. D., & Waskell, L. (1993) *Biochemistry 32*, 8329−8340.
Guiles, R. D., Sarma, S., DiGate, R. J., Banville, D., Basus, V. J., Kuntz, I. D., & Waskell, L. (1996) *Nat. Struct. Biol. 3*, 333−339.
Güntert, P., Braun, W., & Wüthrich, K. (1991) *J. Mol. Biol. 217*, 517−530.
Horrocks, W. D., Jr., & Hall, D. D. (1971) *Coord. Chem. Rev. 6*, 147−186.
Hultquist, D. E., Sanes, L. J., & Jackett, D. A. (1984) *Curr. Top. Cell Regul. 24*, 287−300.
Kay, L. E., Marion, D., & Bax, A. (1989) *J. Magn. Reson. 84*, 72−84.
Keepers, J. W., & James, T. L. (1984) *J. Magn. Reson.* 57, 404−426.
Keller, R. M., & Wüthrich, K. (1972) *Biochim. Biophys. Acta 285*, 326−336.
Kricheldorf, H. R. (1981) *Org. Magn. Reson. 15*, 162−177.
Kumar, A., Wüthrich, K., & Ernst, R. R. (1980) *Biochem. Biophys. Res. Commun. 95*, 1−6.
Kunkel, T. A., Roberts, J. D., & Znakour, R. A. (1987) *Methods Enzymol. 154*, 367−382.
La Mar, G. N., Burns, P. D., Jackson, J. T., Smith, K. M., Langry, K. C., & Strittmatter, P. J. (1981) *J. Biol. Chem. 256*, 6075−6079.
Langridge, R., Ferrin, T. E., Kuntz, I. D., & Connolly, M. L. (1992) *Science 258*, 1740−1741.
Lee, K.-B., La Mar, G. N., Kehres, L. A., Fujinari, E. M., Smith, K. M., Pochapsky, T. C., & Sligar, S. G. (1990) *Biochemistry 29*, 9623−9631.
Lee, K.-B., La Mar, G. N., Mansfield, K. E., Smith, K, M., Pochapsky, T. C., & Sligar, S. G. (1993) *Biochim. Biophys. Acta 1202*, 189−199.
Marion, D., & Wüthrich, K. (1983) *Biochem. Biophys. Res. Commun. 113*, 967−974.
Marion, D., Kay, L. E., Sparks, S. W., Torchia, D. A., & Bax, A. (1989a) *J. Am. Chem. Soc. 111*, 1515−1517.
Marion, D., Driscoll, P. C., Kay, L. E., Wingfield, P. T., Bax, A., Gronenborn, A. M., & Clore, G. M. (1989b) *Biochemistry 28*, 6150−6156.
Mathews, F. S. (1985) *Prog. Biophys. Mol. Biol. 45*, 1 −56.
Mathews, F. S., Czerwinski, E. W., & Argos, P. (1979) in *The Porpyrins* (Dolphin, D., Ed.) Vol. VIIB, pp 107−147, Academic Press, New York.
McIntosh, L. P., Griffey, R. H., Muchmore, D. C., Nielson, C. P., Redfield, A. G., & Dahlquist, F. W (1987) *Proc. Natl. Acad. Sci. U.S.A. 84*, 1244−1248.
McLachlan, S. J., La Mar, G. N., & Lee, K.-B. (1988) *Biochim. Biophys. Acta 957*, 430−445.
Moore, G. R., & Pettigrew, G. W. (1990) *Cytochrome c. Evolutionary, Structural and Physicochemical Aspects*, Springer-Verlag, Berlin.
Neuhaus, D., & Williamson, M. P. (1989) *The Nuclear Overhauser Effect in Structural and Conformational Analysis*, pp 73−85, VCH Publishers, New York.
Nirmala, N., & Wagner, G. (1988) *J. Am. Chem. Soc. 110*, 7557−7558.
Palmer, A. G., III, Rance, M., & Wright, P. E. (1991) *J. Am. Chem. Soc. 113*, 4371−4380.
Perutz, M. F. (1989) *Q. Rev. Biophys. 22*, 139−236.
Piantini, U., Sørenson, O. W., & Ernst, R. R. (1982) *J. Am. Chem. Soc. 104*, 6800−6801.
Pochapsky, T. C., Sligar, S. G., McLachlan, S. J., & La Mar, G. N. (1990) *J. Am. Chem. Soc. 112*, 5258−5263.
Rajarathnam, K., Qin, J., La Mar, G. N., Chiu, M. L., & Sligar, S. G. (1993) *Biochemistry 32*, 5670−5680.
Safo, M. F., Gupta, G. P., Walker, F. A., & Scheidt, R. W. (1991) *J. Am. Chem. Soc. 113*, 5497−5510.
Saiki, R. K., Gelfand, D. H., Stoffel, S., Scharf, S. J., Higuchi, R., Horn, G. T., Mullis, K. B., & Erlich, H. A. (1988) *Science 239*, 478−494.
Sanger, F. S., Nickelson, S., & Coulson, A. R. (1977) *Proc. Natl. Acad. Sci. U.S.A. 74*, 5463−5467.
Sarma, S., DiGate, R. J., Goodin, D. B., Miller, C. J., & Guiles, R. D. (1997) *Biochemistry 36*, 5658−5668.
Scheidt, W. R., & Chipman, D. M. (1986) *J. Am. Chem. Soc. 108*, 163−167.
Shaka, A. J., Keeler, J., & Freeman, R. (1983) *J. Magn. Reson. 53*, 313−340.
Shuker, S. B., Hajduk, P. J., Meadows, R. P., & Fesik, S. W. (1996) *Science 274*, 1531−1534.
Smith, S. O., Farr-Jones, S., Griffin, R. G., & Bachovchin, W. W. (1989) *Science 244*, 961−964.
States, D. J., Habekorn, R. A., & Ruben, D. J. (1982) *J. Magn. Reson. 48*, 286−292.
Strittmatter, P., & Velick, S. F. (1956) *J. Biol. Chem. 221*, 253−264.
Studier, F. W., Rosenberg, A. H., & Dunn, J. J. (1990) *Methods Enzymol. 185*, 113−350.
Veitch, N. C., Whitford, D., & Williams, R. J. P. (1990) *FEBS Lett. 269*, 297−304.
von Bodman, S. B., Schulder, M. A., Jollie, D. R., & Sligar, S. G. (1986) *Proc. Natl. Acad. Sci. U.S.A. 83*, 9433−9447.
Walker, A. F., Huynh, B. H., Scheidt, R. W., & Osvath, S. R. (1986) *J. Am. Chem. Soc. 108*, 5288−5297.
Walker, A. F., Emrick, D., Rivera, J. E., Hanquet, B. J., & Buttlaire, D. H. (1988) *J. Am. Chem. Soc. 110*, 6234−6240.
Weisbluth, M. (1976) *Struct. Bonding 2*, 84−90.

BI961858X